RAPID COMMUNICATIONS

PHYSICAL REVIEW B **95**, 121409(R) (2017)

# Waveguide photonic limiters based on topologically protected resonant modes

U. Kuhl,[1] F. Mortessagne,[1] E. Makri,[2] I. Vitebskiy,[3] and T. Kottos[2]

[1]*Institut de Physique de Nice, Université Côte d'Azur, CNRS, F-06100 Nice, France*

[2]*Department of Physics, Wesleyan University, Middletown, Connecticut 06459, USA*

[3]*Air Force Research Laboratory, Sensors Directorate, Wright-Patterson Air Force Base, Ohio 45433, USA*

(Received 1 May 2016; revised manuscript received 25 February 2017; published 29 March 2017)

We propose a concept of chiral photonic limiters utilizing topologically protected localized midgap defect states in a photonic waveguide. The chiral symmetry alleviates the effects of structural imperfections and guarantees a high level of resonant transmission for low intensity radiation. At high intensity, the light-induced absorption can suppress the localized modes, along with the resonant transmission. In this case the entire photonic structure becomes highly reflective within a broad frequency range, thus increasing dramatically the damage threshold of the limiter. Here, we demonstrate experimentally the loss-induced reflection principle of operation which is at the heart of reflective photonic limiters using a waveguide consisting of coupled dielectric microwave resonators.

DOI: 10.1103/PhysRevB.95.121409

The emerging field of topological photonics aims to realize photonic structures which are resilient to fabrication imperfections [1–10]. Usually, these structures, support topologically protected (TP) defect states within photonic band gaps. In this endeavor the manipulation of various symmetries has been proven extremely useful. An example case are resonator arrays with chiral symmetry [11] where a topological defect state appears to be insensitive to positional imperfections of the resonators [11,12]. In this Rapid Communication we connected the chiral symmetric array to leads, thus turning the TP defect mode to a *quasilocalized resonant mode* which was utilized for the realization of a topologically protected class of waveguide photonic limiters.

Limiters are protecting filters transmitting low-power (or energy) input signals while blocking the signals of excessively high power (or energy) [13–18]. Usually, a passive limiter absorbs the high-level radiation, which can cause its overheating. The input level above which the transmitted signal intensity does not grow with the input is the limiting threshold (LT). Another important characteristic is the limiter damage threshold (LDT), above which the limiter sustains irreversible damage. The domain between LT and LDT is the dynamic range (DR) of the limiter—the larger it is, the better. Unfortunately, material limitations impose severe restrictions on both thresholds. Importantly, these structures should be tolerant to deviation of the material and geometrical parameters from their ideal values.

Along these lines, the defect modes hosted by photonic band-gap [16,19–21] (or other resonant [22]) structures have been exploited as an alternative to achieve flexible, high efficiency photonic limiters. In most occasions, however, limiting action is achieved by a nonlinear frequency shift of the transparency window of the photonic structure. Such a shift is inherently small and, therefore, cannot provide broadband protection from high-power input. Other schemes, specifically in the microwave domain, exploit PIN diode (having spike leakage problems) [23], transmitter-receiver (TR) tubes, or self-attenuating superconducting transmission lines that require high-power consumption [24]. To address these issues we have recently proposed the concept of *reflective photonic limiters* [25,26]. Such limiters reflect the high radiation, thereby protecting themselves—not just the receiving device—while they provide a strong resonant transmission for low incident radiation.

Here, we propose the use of chiral coupled resonator waveguides (C-CROWs) with alternating short and long distances from one another (see Fig. 1), as a fertile platform to implement structurally robust reflective waveguide limiters with a wide DR. In the presence of a phase slip defect [27,28], chiral symmetry provides topological protection to a midgap defect localized mode [11,12]. For low incident power (or energy) it can provide high transmittance shielded from (positional) fabrication imperfections. When (nonlinear) losses at the defect resonator (triggered from high-power, or energy, incident radiation) exceed a critical value, the resonant defect mode and the associated resonant transmission are dramatically suppressed, turning the C-CROW highly reflective (not absorptive) for a *broad frequency range*. As a result, the LDT increases with a consequent increase of the DR of the limiter. Using a microwave C-CROW arrangement we have tested experimentally the operational principle of this class of TP reflective photonic limiter by investigating the sensitivity and transport characteristics of the TP *resonant* defect mode in the presence of losses and imperfections.

The setup [see Fig. 1(a)] consists of $N = 21$ high index cylindrical resonators (radius $r = 4$ mm, height $h = 5$ mm, made of ceramics with refraction index $n \approx 6$) with an eigenfrequency around $\nu_0 = 6.655$ GHz and linewidth $\gamma = 1.4$ MHz [29]. The resonators are placed at alternating distances $d_1 = 12$ mm and $d_2 = 14$ mm corresponding to strong ($t_1 = 38$ MHz) and weak ($t_2 = 21$ MHz) evanescent couplings, respectively. A topological defect at the 11th resonator is introduced by repeating the spacing $d_2$ [11,12]. Close to the first resonator, we have placed a kink antenna that emits a signal exciting the first transverse electric ($TE_1$) resonant mode of the resonators. The structure is shielded from above with a metallic plate where a movable loop antenna (receiving antenna) is mounted and is coupled to the 13th resonator [29].

We assume that the defect resonator incorporates a nonlinear absorption mechanism, i.e., we assume that its losses are self-regulated depending on the strength of the incident radiation. One option to incorporate nonlinear losses is via an external element (fast diodes) [see Fig. 1(b)]. This option

 

RAPID COMMUNICATIONS



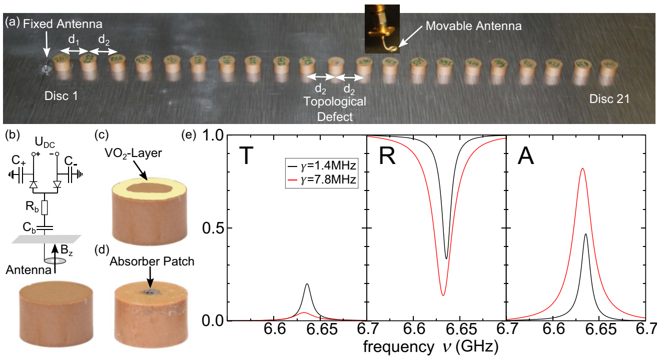


FIG. 1. (a) The experimental setup: The resonators are separated by distances $d_1$ or $d_2$ with $d_1 < d_2$. A central defect is introduced by repeating the spacing $d_2$. Various proposals for the implementation of nonlinear losses in the defect resonator: (b) A circuit with various module (sensing antenna, diode, threshold DC voltage). (c) An epitaxial growth of a material that experiences a thermally induced insulator-to-metal phase transition. (d) Our measurements involve a defect resonator, which includes a manually modulated absorbing patch. (e) Measured transmittance $T$, reflectance $R$, and absorption $A$ for two different patches. The linewidth $\gamma$ (1.4 and 7.8 MHz) of the reflected signal mainly characterizes the losses due to the absorbing patches.

provides on-the-fly reconfigurability of the LT via an externally tuned DC voltage $U_{\mathrm{DC}}$. An alternative mechanism is associated with temperature driven insulator-to-metal phase transition materials, such as $VO_2$ [30–33], which can be deposited on top of the defect resonator [see Fig. 1(c)].

In our experiment we are not concerned with the physical origin of the nonlinear losses at the defect resonator. Rather, we focus on demonstrating their effects on the transport properties of the photonic structure and how can be utilized for microwave limiters. Therefore, we have included losses $\gamma_D$ by placing an absorbing patch on top of the resonator [see Fig. 1(d)]. This process results in a slight shift of the real part of the permittivity of the defect resonator, which we corrected by using resonators with a slightly higher eigenfrequency. The linewidth $\gamma$ has been used in order to quantify the losses of the resonators.

In Fig. 1(e) we show the transmittance $T$, reflectance $R$, and absorption $A = 1 - T - R$ for two resonators with different losses. We observe that the transmittance of the standalone lossy resonator reduces as the losses increase, thus acting as a limiter. However, this reduction comes to the expense of increasing absorption, i.e., *the standalone lossy resonator acts as a sacrificial limiter*.

The photonic structure is described by a one-dimensional (1D) tight-binding Hamiltonian [34]

$$H_P = \sum_n \nu_n |n\rangle\langle n| + \sum_n t_n(|n\rangle\langle n+1| + |n+1\rangle\langle n|, \quad (1)$$

where $n = 1,2,\ldots,21$ enumerates the resonators, $\nu_n = \nu = \nu_0 - i\gamma$ is the resonance frequency of the $n$th resonator, and $t_n$ ($= t_1$ or $t_2$) is the coupling between nearest resonators. The band structure consists of two minibands $\nu_0 - t_1 - t_2 < \nu < \nu_0 - |t_1 - t_2|$ and $\nu_0 + |t_1 - t_2| < \nu < \nu_0 + t_1 + t_2$ separated by a finite gap of width $2|t_1 - t_2|$. In the presence of the defect resonator at $n_0 = 11$, a TP defect mode at $\nu_D = \nu_0$ [11,12] is created. Its shape, in the limit of infinite many resonators, is [11]

$$\psi_n^D \sim \begin{cases} \frac{1}{\sqrt{\xi}} e^{-|n-n_0|/\xi}, & n \text{ odd}, \\ 0, & n \text{ even}, \end{cases} \quad (2)$$

where $\psi_n^D$ is the amplitude of the defect mode at the $n$th resonator and $\xi = 1/\ln(t_1/t_2)$ is the so-called localization length of the mode [11]. Hamiltonian Eq. (1) is invariant under a chiral symmetry, i.e., $\{H_P, C\} = 0$ where $\{\cdots\}$ indicates an anticommutation and $C = P_{\mathrm{even}} - P_{\mathrm{odd}}$ with $C^2 = 1$ ($P_{\mathrm{even/odd}}$ is the projection operator in the even/odd sites). The staggering form of $\psi^D$ is a consequence of the chiral symmetry [11,12].

We are modeling the transmitted (reflected) antenna, coupled to the $n_T = 1$ ($n_R = 13$) resonator, by a 1D semi-infinite tight-binding lattice with coupling constant $t_L = (t_1 + t_2)/2$ and on-site energies $\nu_L = \nu_0$. The associated scattering matrix takes the form [35]

$$\hat{S} = -\hat{1} + \frac{2i \sin k}{t_L} W^T \frac{1}{H_{\mathrm{eff}} - \nu} W, \quad H_{\mathrm{eff}} = H_P + \frac{e^{ik}}{t_L} W W^T, \quad (3)$$

where $\hat{1}$ is the $2 \times 2$ identity matrix, $W_{nm} = w_T \delta_{n,n_T}\delta_{m,1} + w_R \delta_{n,n_R}\delta_{m,2}$ is a $N \times 2$ matrix that describes the coupling between the array and the antennas, $\nu = \nu_L + 2t_L \cos k$ is the frequency of propagating waves at the antennas, and $k$ is their associated wave vector.

When the system is coupled to the antennas, $\psi^D$ becomes a quasilocalized resonant mode at frequency $\nu_D \approx \nu_0$, with a large but finite lifetime $\tau$,

$$\tau^{-1} \sim \left\langle \psi^D \middle| \frac{e^{ik}}{t_L} W W^T \middle| \psi^D \right\rangle = |w_T|^2 |\psi_1^D|^2 + |w_R|^2 |\psi_{13}^D|^2, \quad (4)$$

where $|\psi_1^D|^2, |\psi_{13}^D|^2$ are given by Eq. (2).

The measured transmittance $T = |S_{12}|^2$, reflectance $R = |S_{11}|^2$, and absorption $A = 1 - T - R$ versus frequencies $\nu$ of the C-CROW (with global $\gamma = 1.4$ MHz $= \gamma_D$) are shown in Figs. 2(a)–2(c) (solid lines). Measurements of the widths of the minibands and of the gap allow us to extract the couplings $t_1 = 38$ MHz, $t_2 = 21$ MHz. The presence of the defect resonator results in a transmission peak at $\nu = \nu_D$ inside the band gap. A fitting of the height of this peak, for various $\gamma_D$ values, gives $w_T = 10.915$ MHz, $w_R = 3.6875$ MHz (see Fig. 3). The small peak in the absorption [solid line in Fig. 2(c)] is associated with the small ohmic component at all resonators. In Fig. 2(a) we also report (dashed lines) the measured transmittance for a defect with additional losses, i.e., $\gamma_D = 7.8$ MHz. We find that even a small increase in $\gamma_D$ strongly suppresses the resonant transmission [see Fig. 2(a)].

In Fig. 2(b) we show $R(\nu)$ of the C-CROW for $\gamma_D = 1.4$ MHz (solid line) and $\gamma_D = 7.8$ MHz (dashed line). We find that the suppression in $T(\nu_D)$ is accompanied by an increase in $R(\nu_D)$. Moreover, $A(\nu_D)$ is decreasing as $\gamma_D$ increases [see Fig. 2(c)]. In other words, our photonic structure becomes *reflective* (not absorptive) as the losses of the defect resonator increase. This behavior is in distinct contrast to the case of a single (sacrificial) lossy resonator [see Fig. 1(e)] where the drop in transmittance is associated with an increase of

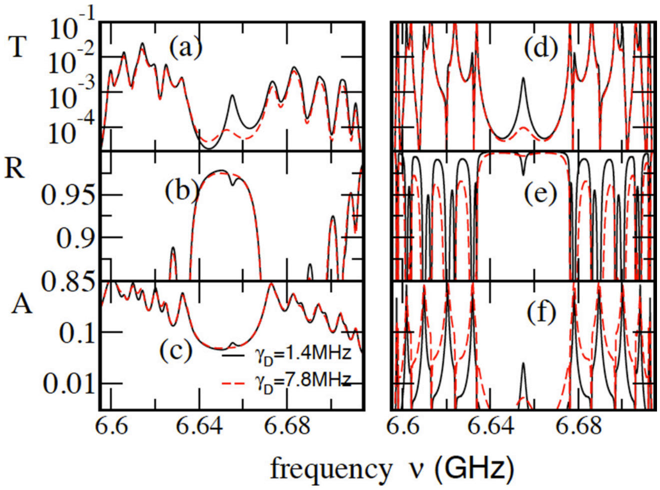


FIG. 2. Measurements of the (a) transmittance $T$, (b) reflectance $R$, and (c) absorption $A$ for the C-CROW of Fig. 1. We considered two different values of $\gamma_D = 1.4$ and 7.8 MHz. All other resonators have $\gamma = 1.4$ MHz. Simulations for (d) $T$, (e) $R$, and (f) $A$ of a C-CROW with lossless resonators ($\gamma = 0$) apart from the defect resonator which has $\gamma_D = 1.4$ MHz (solid lines) and $\gamma_D = 7.8$ MHz (dashed lines).

absorption. These features are also observed in the simulations of an ideal C-CROW where all resonators have zero intrinsic losses $\gamma = 0$ [see Figs. 2(d)–2(f)].

An overview of the measured (black circles) $T(\nu_D)$, $A(\nu_D)$ and the corresponding numerical results (black solid lines) for the C-CROW of Fig. 1 versus $\gamma_D$ are reported at the left column of Fig. 3. We find that an increase of $\gamma_D$ leads to a decrease of $T(\nu_D)$ and $A(\nu_D)$ of the photonic structure. This behavior is contrasted with the measurements (diamonds) and numerics (dashed-dotted lines) of a standalone lossy resonator where we observe relatively large $T$ values $T \sim 10^{-1}$ as opposed to $T \sim 10^{-4}$ for the C-CROW, i.e., ultralow LT. For moderate $\gamma_D$ values the absorption of the standalone resonator reaches large

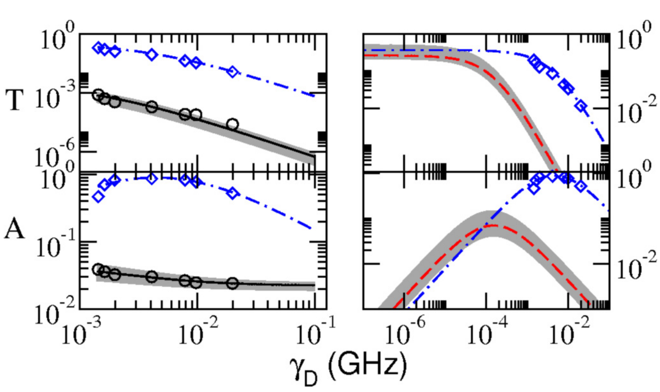


FIG. 3. The transmittance $T$ (up) and absorption $A$ (down) vs $\gamma_D$. Left: For the C-CROW with resonator losses $\gamma = 1.4$ MHz (black lines, numerics; circles, experiment) and for the standalone resonator (blue dashed-dotted lines, numerics; diamonds, experiment). Right: Numerics for the ideal C-CROW (red dashed lines) with $\gamma = 0$ at all other resonators. Symbols (blue dashed-dotted lines) correspond to measurements (numerics) of $T$ and $A$ for the standalone resonator. Shadowed areas indicate deviations in $T, A$ due to randomness in the couplings.

values $A(\gamma_D = 0.004 \text{ GHz}) \approx 0.8$ corresponding to low LDT. In contrast, the C-CROW takes absorption values, which are at least one order of magnitude smaller (high LDT). On the right column of Fig. 3, we report the simulations for $T(\nu_D)$, $A(\nu_D)$ for an ideal ($\gamma = 0$) C-CROW (dashed lines) versus the losses $\gamma_D$ of the defect resonator. These results are compared to the theoretical/experimental (dashed-dotted lines/diamonds) results for the standalone lossy resonator. Both cases show the same qualitative behavior. However, the C-CROW shows a two-order lower LT (i.e., a smaller $\gamma_D$ value for which the decay of transmittance occurs) as compared to a standalone resonator. At the same time the LDT of the C-CROW is at least two orders of magnitude higher than the one associated with the standalone resonator. The latter acquires a maximum value of absorption $A \approx 0.8$ at $\gamma_D \approx 0.01$ as opposed to $A \approx 0.01$ acquired by the C-CROW. The maximum absorption for the photonic structure occurs at much lower values of $\gamma_D \sim 10^{-4}$, which in the case of a nonlinear lossy mechanism corresponds to rather small, and therefore harmless, incident radiation.

The transport features of the TP resonant mode have been further investigated in the case of positional randomness corresponding to a box distribution for the coupling constants $\tilde{t}_{1,2} \in [t_{1,2} - 2 \text{ MHz}, t_{1,2} + 2 \text{ MHz}]$. The shadowed area in Fig. 3 indicates the variations in $T, A$. For $\gamma_D \approx 0$ (not shown) the resonant frequency $\nu_0 \approx 6.655$ GHz remains protected and the resonant transmission is unaffected for both an ideal C-CROW $\gamma = 0$ and for resonators with losses $\gamma = 1.4$ MHz. Moreover, the experimental data in Fig. 3 incorporate an intrinsic disorder associated with the variation of the bare resonance frequencies, within a range of 1 MHz, and the precision of the resonator positioning, of the order of 0.2 mm (coupling uncertainty $\approx$ 500 kHz). Nevertheless, the transport features remain largely unaffected (see Fig. 3).

The fragility of the resonant defect mode is further analyzed in Fig. 4. In Fig. 4(a) we report the simulated resonant defect fields for an ideal C-CROW (i.e., $\gamma = 0$) and for various $\gamma_D$ values. For $\gamma_D = 0$, a nice agreement between the numerics and Eq. (2) is observed, indicating that the coupling to the antennas does not affect the resonant mode profile. As $\gamma_D$ increases, a gradual deviation from the profile of Eq. (2) occurs and eventually a suppression of the defect mode is observed.

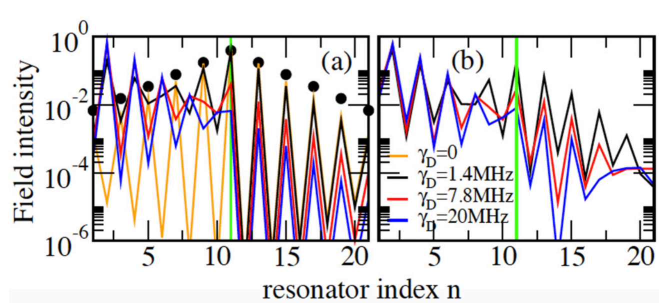


FIG. 4. (a) Simulations for an ideal C-CROW consisting of resonators with $\gamma = 0$. Solid black circles correspond to Eq. (2) for the defect mode profile. Solid lines correspond to the simulations of the resonant defect mode profile for various $\gamma_D$. For symmetry reasons we assumed that the antennas are coupled to the first and last resonator. (b) Experimental resonant mode profiles for various $\gamma_D$ values. The measured losses at all resonators are $\gamma = 1.4$ MHz.

At $\gamma_D = 20$ MHz the resonant localized mode is suppressed enough so that the field intensity in the vicinity of the defect lossy resonator is two orders smaller than the corresponding one for $\gamma_D = 0$. *Thus the lossy defect resonator is protected from damages induced by heat or electrical breakdown.* This implies a huge increase in the DR of C-CROW. The comparison with the experimental data [see Fig. 4(b)], where $\gamma = 1.4$ MHz, indicates that the underlying mechanism which is responsible for the destruction of the resonant defect mode remains unaffected.

The destruction of the resonant defect mode can be understood intuitively as a result of a competition between two mechanisms that control the dwell time of photons in the resonant state. The first one is associated with the boundary losses due to the coupling of the photonic structure to the antennas. It results in a resonant linewidth $\Gamma_{\rm edge} \sim \tau^{-1}$ [see Eq. (4)]. The other mechanism is associated with bulk losses and it leads to an additional broadening of the resonance linewidth. From first-order perturbation theory, $\Gamma_{\rm bulk} \approx \gamma_D|\psi_{11}|^2 + \gamma \sum_{n\neq 11} |\psi_n|^2 = (\gamma_D - \gamma)/\xi + \gamma$. For small values of $\gamma_D$ such that $\Gamma_{\rm bulk} < \Gamma_{\rm edge}$, the dwell time is determined by $\Gamma_{\rm edge}$ and it is essentially constant. Thus the absorption of the photons that populate the resonant state increases, as they are trapped for a relatively long time in the lossy C-CROW [see the peak of the black line in Fig. 2(c)]. When $\Gamma_{\rm bulk} \approx \Gamma_{\rm edge}$, the dwell time itself begins to diminish, and the resonant mode is spoiled. For even larger values of $\gamma_D$ the photons do not dwell at all in the resonant state and reflection from the whole structure becomes the dominant mechanism. As a result, the absorption decreases to zero. The above argumentation applies equally well for the standalone defect and for the photonic structure. However, in the latter case the condition for the destruction of the resonant mode $\Gamma_{\rm bulk} \approx \Gamma_{\rm edge}$ is achieved for *exponentially* smaller values of $\gamma_D$. It is exactly this effect that our proposal is harvesting in order to increase the damaging threshold (and the DR) of the photonic waveguide limiter.

We acknowledge partial support from AFOSR via MURI Grant No. FA9550-14-1-0037 (T.K.) and LRIR14RY14COR (I.V.). E.M. acknowledges partial support from Wesleyan University and from NSF EFMA-1641109. The stay of (T.K.) at LPMC-CNRS was supported by CNRS.

[1] L. Lu, J. D. Joannopoulos, and M. Soljačić, Nat. Phot. **8**, 821 (2014).
[2] S. Raghu and F. D. M. Haldane, Phys. Rev. A **78**, 033834 (2008).
[3] Z. Wang, Y. Chong, J. D. Joannopoulos, and M. Soljacic, Nature (London) **461**, 772 (2009).
[4] M. Hafezi, E. A. Demler, M. D. Lukin, and J. M. Taylor, Nat. Phys. **7**, 907 (2011).
[5] K. Fang, Z. Yu, and S. Fan, Nat. Photonics **6**, 782 (2012).
[6] T. Kitagawa, M. A. Broome, A. Fedrizzi, M. S. Rudner, E. Berg, I. Kassal, A. Aspuru-Guzik, E. Demler, and A. G. White, Nat. Commun. **3**, 882 (2012).
[7] A. B. Khanikaev, S. H. Mousavi, W.-K. Tse, M. Kargarin, A. H. MacDonald, and G. Shvets, Nat. Mater. **12**, 233 (2013).
[8] M. Hafezi, S. Mittal, J. Fan, A. Migdall, and J. M. Taylor, Nat. Photonics **7**, 1001 (2013).
[9] M. C. Rechtsman, J. M. Zeuner, Y. Plotnik, Y. Lumer, D. Podolsky, F. Dreisow, S. Nolte, M. Segev, and A. Szameit, Nature (London) **496**, 196 (2013).
[10] S. Malzard, C. Poli, and H. Schomerus, Phys. Rev. Lett. **115**, 200402 (2015).
[11] J. K. Asbóth, L. Oroszlány, and A. Pályi, *A Short Course on Topological Insulators*, Lecture Notes in Physics Vol. 919 (Cambridge University Press, Cambridge, U.K., 2016).
[12] C. Poli, M. Bellec, U. Kuhl, F. Mortessagne, and H. Schomerus, Nat. Commun. **6**, 6710 (2015).
[13] L. W. Tutt and T. F. Boggess, Prog. Quantum Electron. **17**, 299 (1993).
[14] A. E. Siegman, Appl. Opt. **1**, 739 (1962).
[15] J. E. Geusic, S. Singh, D. W. Tipping, and T. C. Rich, Phys. Rev. Lett. **19**, 1126 (1967).
[16] M. Scalora, J. P. Dowling, C. M. Bowden, and M. J. Bloemer, Phys. Rev. Lett. **73**, 1368 (1994).
[17] T. F. Boggess, S. C. Moss, I. W. Boyd, and A. L. Smirl, Opt. Lett. **9**, 291 (1984).
[18] M. Heinrich, F. Eilenberger, R. Keil, F. Dreisow, E. Suran, F. Louradour, A. Tünnermann, T. Pertsch, S. Nolte, and A. Szameit, Opt. Express **20**, 27299 (2012).
[19] B. Y. Soon, J. W. Haus, M. Scalora, and C. Sibilia, Opt. Express **11**, 2007 (2003).
[20] M. Larciprete, C. Sibilia, S. Paoloni, M. Bertolotti, F. Sarto, and M. Scalora, J. Appl. Phys. **93**, 5013 (2003).
[21] X. Liu, J. W. Haus, and M. S. Shahriar, Opt. Express **17**, 2696 (2009).
[22] L. W. Cross, M. J. Almalkawi, and V. K. Devabhaktuni, IEEE Trans. Electromagn. Compat. **55**, 1100 (2013).
[23] R. V. Garver, *Microwave Diode Control Devices* (Artech House, Norwood, MA, 1976).
[24] J. C. Booth, D. A. Rudman, and R. H. Ono, IEEE Trans. Appl. Supercond. **13**, 305 (2003).
[25] E. Makri, H. Ramezani, T. Kottos, and I. Vitebskiy, Phys. Rev. A **89**, 031802(R) (2014).
[26] E. Makri, T. Kottos, and I. Vitebskiy, Phys. Rev. A **91**, 043838 (2015).
[27] V. M. Apalkov and M. E. Raikh, Phys. Rev. Lett. **90**, 253901 (2003); E. A. Avrutin and M. E. Raikh, Sov. Phys. – Tech. Phys. **33**, 1170 (1988).
[28] J. S. Foresi, P. R. Villeneuve, J. Ferrera, E. R. Thoen, G. Steinmeyer, S. Fan, J. D. Joannopoulos, L. C. Kimerling, H. I. Smith, and E. P. Ippen, Nature (London) **390**, 143 (1997).
[29] M. Bellec, U. Kuhl, G. Montambaux, and F. Mortessagne, Phys. Rev. B **88**, 115437 (2013).
[30] J. H. Bechtel and W. L. Smith, Phys. Rev. B **13**, 3515 (1976).
[31] A. Crunteanu, J. Givernaud, P. Blondy, J.-C. Orlianges, C. Champeaux, and A. Catherinot, in *Advanced Microwave and Millimeter Wave Technologies Semiconductor Devices Circuits and Systems*, edited M. Mukherjee (InTech, Rijeka, Croatia, 2004), Chap. 3, pp. 35–56.

[32] P. Phoempoon and L. Sikong, Sci. World J. **2014**, 841418 (2014).

[33] A. L. Pergament, G. B. Stefanovich, N. A. Kuldin, and A. A. Velichko, ISRN Condens. Matter Phys. **2013**, 960627 (2013).

[34] P. Markos and C. M. Soukoulis, *Wave Propagation: From Electrons to Photonic Crystals and Left-Handed Materials* (Princeton University Press, Princeton, NJ, 2008).

[35] S. Datta, *Electronic Transport in Mesoscopic Systems* (Cambridge University Press, Cambridge, U.K., 1995).